Published in final edited form as:
Adv Mater. 2013 January 11; 25(2): 227–232. doi:10.1002/adma.201202932.

Plasmid-Templated Shape Control of Condensed DNA–Block Copolymer Nanoparticles

Dr. Xuan Jiang[#],
Department of Materials Science and Engineering, Whiting School of Engineering, Johns Hopkins University, Baltimore, Maryland 21218; Translational Tissue Engineering Center and Whitaker Biomedical Engineering Institute, Johns Hopkins School of Medicine, Baltimore, Maryland 21287, USA

Wei Qu[#],
Department of Materials Science and Engineering, Northwestern University, Evanston, Illinois 60208, USA

Deng Pan,
Department of Biomedical Engineering, Johns Hopkins School of Medicine, Baltimore, Maryland 21205, USA

Dr. Yong Ren,
Department of Materials Science and Engineering, Whiting School of Engineering, Johns Hopkins University, Baltimore, Maryland 21218, USA

John-Michael Williford,
Department of Biomedical Engineering, Johns Hopkins School of Medicine, Baltimore, Maryland 21205, USA

Professor Honggang Cui,
Department of Chemical and Biomolecular Engineering, Whiting School of Engineering, Johns Hopkins University, Baltimore, Maryland 21218, USA

Professor Erik Luijten, and
Department of Materials Science and Engineering, Northwestern University, Evanston, Illinois 60208; Department of Engineering Sciences and Applied Mathematics, Northwestern University, Evanston, Illinois 60208, USA

Professor Hai-Quan Mao
Department of Materials Science and Engineering, Whiting School of Engineering, Johns Hopkins University, Baltimore, Maryland 21218; Translational Tissue Engineering Center and Whitaker Biomedical Engineering Institute, Johns Hopkins School of Medicine, Baltimore, Maryland 21287, USA

Erik Luijten: luijten@northwestern.edu; Hai-Quan Mao: hmao@jhu.edu

Keywords

plasmid DNA; templated self-assembly; shape control; solvent polarity; gene delivery

Plasmid condensation by cationic polymers in aqueous solutions has been widely used to prepare DNA nanoparticles with diameters ranging from tens to hundreds of nanometers.[1]

Correspondence to: Erik Luijten, luijten@northwestern.edu; Hai-Quan Mao, hmao@jhu.edu.
[#]These authors contributed equally to this work.

Although many of these polycation–DNA nanoparticles display relatively high levels of transfection efficiency in cell culture, their performance *in vivo* has been disappointing.[2] This low *in vivo* delivery efficiency partly results from insufficient control over the physical properties and colloidal stability of the nanoparticles. Several methods have been developed to improve colloidal stability of DNA nanoparticles in physiological media, including polyethylene glycol (PEG)-conjugation, polyionic coating, and condensing DNA into polyelectrolyte micelles.[3] However, until now there has been no effective method to *control* and *tune* the shape of plasmid DNA-containing nanoparticles within this size range. This limitation is particularly pressing in view of several recent studies that show the importance of nanoparticle shape in regulating their cellular uptake and *in vivo* transport,[4–6] as demonstrated for the uptake of gold nanoparticles by macrophages,[7] for margination dynamics of nanoparticles in blood vessels,[6] and for the tissue distribution and circulation stability and thus drug delivery efficiency of organic and inorganic nanoparticles.[5,8] We note that none of these shaped nanoparticles have been used to package and deliver plasmid DNA.

Here, we report a new method for tuning plasmid DNA nanoparticles by varying solvent polarity during the condensation of DNA with PEG-*b*-polyphosphoramidate (PPA)[9,10] (Fig. 1). Upon separately dissolving the copolymer (Fig. S1 and Table S1) and plasmid DNA in dimethylformamide (DMF)–water mixtures at fixed volumetric ratios and mixing the two solutions at a predetermined copolymer-to-DNA ratio to achieve effective DNA condensation,[11] we have observed a striking variation in morphology (Fig. 1b–e). Micelles formed in pure water assumed a mixture of long worm- and ring-like morphologies (Fig. 1b). In a 3:7 (v/v) DMF–water mixture, a small fraction of spherical and rod-like micelles appeared among the dominant worm-like structures (Fig. 1c) with lengths shorter than those observed in water. When the DMF/water volumetric ratio was increased to 5:5, more than 90% of the micelles adopted a uniform, rod-like morphology (Fig. 1d) with a diameter of 24 ± 3 nm and a length of 70 ± 10 nm. Additionally, we observed a small population of spherical micelles with a diameter of 41 ± 7 nm. Further increase in the DMF/water volumetric ratio to 7:3 led to formation of highly uniform spherical micelles with a diameter of 40 ± 5 nm (Fig. 1e). These structures were confirmed using cryogenic TEM imaging (Fig. S2). This method of generating DNA-compacting micelles with different shapes is not limited to DMF as a co-solvent; we have successfully prepared a series of analogous micelles using dimethyl sulfoxide (DMSO)–water solvent mixtures (Fig. S3).

To gain insight into the mechanism of this dramatic variation in micelle shape, we performed molecular dynamics simulations of a coarse-grained anionic semiflexible ring polyelectrolyte (representing the plasmid DNA) in the presence of neutral–cationic block copolymer (representing PEG-*b*-PPA). This modeling approach explicitly incorporates fluctuation effects, while all electrostatic interactions are accurately taken into account using Ewald summation.[12–14] The detailed molecular parameters chosen to model the experimental system are described in the Supporting Information (Section 2). Since we employed an implicit solvent, the variation of DMF–water ratio, and hence solvent polarity, was modeled by tuning the polymer interaction parameters, DNA charge density, and the dielectric constant, as summarized in four representative parameter sets (referred to as Solvents 1 to 4, Table S3). As illustrated in Fig. 1f–i, in all cases we observed copolymer/DNA complexation, but with an increasingly compact morphology reflecting the conformational changes of the condensed plasmid DNA in the micelle core. Decreasing the solvent polarity (corresponding to an increase in DMF–water ratio) to obtain Solvents 1 through 4, we observed that the shape of the micelles progressively changed from worm-like chains coexisting with toroidal structures to a folded rod-like morphology, and then to a compact spherical structure. These shape changes are in excellent agreement with those

observed in Fig. 1b–e and demonstrate how the plasmid DNA acts as a template for the micellar nanoparticles.

The molecular dynamics simulations also make it possible to quantify shape fluctuations and the relative probability of various morphologies at different solvent conditions. To this end we considered the eigenvalues λ_i (i = 1, 2, 3) of the radius-of-gyration tensor of the micelle and computed the ensemble average of the asphericity,[15,16]

$$A=\frac{1}{2}\left\langle \frac{(\lambda_1-\lambda_2)^2+(\lambda_2-\lambda_3)^2+(\lambda_3-\lambda_1)^2}{(\lambda_1+\lambda_2+\lambda_3)^2} \right\rangle,$$

which takes values between 0 (sphere) and 1 (straight rod). Fig. 2 illustrates the predicted frequency distribution of A for the four different model solvent conditions examined, along with representative conformations of the plasmid DNA within the micelle. This analysis shows that for a given solvent polarity there is an inherent distribution of morphologies. As the solvent polarity was gradually decreased from Solvents 1 through 4, the micelles changed from predominantly worm-like, flexible morphologies and some ring-shaped structures to different, well-defined shapes with relatively narrow fluctuations in asphericity. Although there is no direct quantitative mapping of the solvent conditions of Fig. 2 on DMF–water composition, this analysis demonstrates that solvent polarity plays a critical role in determining shape variation and distribution in these assembled micelles.

The agreement between the experimental observations and the molecular simulations provides the basis for describing the formation and shape variation of the micelles via a simple polymer model. Indeed, the initial assembly of these micelles results from the complexation of DNA with PPA blocks, ensuring the compaction of DNA, akin to condensation driven by multivalent counterions,[12,13,17] The electrostatic interactions between DNA and PPA, combined with entropy gain due to counterion release, overcome the entropic losses due to confinement of DNA and PPA and the resulting constraints on the PEG blocks. Subsequent variation of the solvent composition through addition of DMF has multiple effects on the molecular interactions. First, the solubility of DNA is lowered,[18] further promoting the formation of a compact aggregate (Fig. S4). This coil–globule transition does not result in global polymer–solvent phase separation, owing to the low DNA concentration and the presence of a corona of PEG blocks around each DNA/PPA globule. Secondly, both the dielectric constant and the surface charge density of the DNA and PPA decrease. However, the electrostatic interactions are only weakly affected by an increase in DMF–water ratio, since these two effects largely cancel (Table S2). On the other hand, the lower charge density of DNA decreases the entropy gain from counterion release, but this effect is overwhelmed by the lowered DNA solubility.

Thus, the micellar shape variation primarily arises from a competition between DNA solubility and maximization of PEG entropy. To quantify the latter, we make an analogy between the PEG corona and a spherocylindrical (so chosen as to permit smooth interpolation from spherical to elongated shapes) polymer brush with short axis 2h and long axis L+2h, we note that the free energy of the latter is controlled by the number of chains in the brush n, their degree of polymerization N, and the elongation L. The free energy per chain varies from $f \sim kTN^{1/5}(wn/a^3)^{2/5}$ in the spherical limit (L = 0) to $f \sim kTN^{1/2}(wn/a^2L)^{1/2}$ in the elongated limit ($L \rightarrow h$), where kT is the thermal energy, a the Kuhn length and w the excluded-volume parameter.[19] Applying this result to the PEG corona, we observe that changing the DMF–water ratio does not induce a strong variation of a or w, since PEG solubility is only weakly dependent on the solvent composition over the range tested here.

On the other hand, both the PEG block length (*N*) and the net charge of the PPA block, which alters the number of block copolymers (*n*) associated with the DNA, can function as control parameters. Whereas these parameters are held constant in our experiments and simulations, the free energy of the PEG chains in the corona can still be changed through micelle shape variation, crossing over from $f \sim n^{2/5}$ to $f \sim (n/L)^{1/2}$ upon elongation. This tendency of the PEG corona to favor aspherical shapes is counteracted by the strong enthalpic contribution that arises upon increasing the concentration of DMF, a poor solvent for DNA, which pulls the DNA–PPA core and thus also the PEG corona into an increasingly compact shape. The role of PEG is reconfirmed by observations that neither DNA alone (Fig. S4) nor DNA complexed with PPA homopolymer produced comparable shape changes in DMF–water mixtures (Figs. S5 and S7). On the other hand, separate simulations also uncovered that in the absence of DNA bending rigidity the micelles adopted more irregular shapes. Thus, the entire spectrum of morphologies arises from an intricate interplay of DNA–solvent interaction, DNA bending rigidity, and PEG entropy. This analysis is clearly only semi-quantitative in nature. Nevertheless, the good agreement between the simulations and the analytical model confirms a comprehensive understanding of the competing mechanisms at work. Consequently, this model can provide guidance in the choice of various parameters in future experiments.

Since the molecular dynamics simulations examine equilibrium structures, we anticipated the possibility of producing micelles with different shapes by varying solvent polarity *after* their formation. To verify this, we prepared uniform spherical micelles in a 7:3 (v/v) DMF–water mixture as shown in Fig. 1e, and then gradually increased the polarity of the solvent by titrating water into the micelle solution. As the DMF/water volumetric ratio was decreased from 7:3 to 1:9, the assembled micelles reverted to rod- and worm-like morphologies (Fig. 3). Interestingly, the micelles obtained by this solvent-titration method showed an even higher degree of uniformity than those prepared by directly mixing copolymer and DNA under the same solvent condition (Fig. 1). Such a high degree of uniformity of these micelles is remarkable when compared with other block copolymer micelles and may reflect a nonequilibrium distribution resulting from the gradual solvation of the DNA/PPA cores of a uniform initial population of spherical micelles (Fig. 3a).[20] Nevertheless, this is a highly effective method to generate DNA-compacting micelles with distinct and uniform shapes using the same copolymer and the same plasmid DNA, providing a promising platform to explore the effect of shape on their biological activities.

Since transfection experiments must be conducted in aqueous solution, the micellar shapes generated by our approach need to be preserved upon removal of DMF from the solvent mixture. We accomplished this via a reversible disulfide crosslinking method (Figs. S8–10) that we developed previously to stabilize PEG-*b*-PPA/DNA micelles and that was observed to yield prolonged and enhanced transgene expression.[11,21] We confirmed that the micelles maintained their respective shapes after crosslinking and remained stable after solvent exchange to water (Fig. 4a–e) and after incubation in saline (Fig. S11) and 10% serum (Fig. S12). All micelles, ranging from worm- to spherical-shaped, exhibited electrostatically neutral surfaces as demonstrated by near-zero zeta potentials measured in saline (Fig. 4f). As a proof of concept, we examined the shape-dependent transfection efficiency of these shaped nanoparticles in the rat liver following retrograde intrabiliary infusion, since we have established this as the most effective route to achieve liver-targeted gene delivery for polycation/DNA nanoparticles.[10,22] Among these crosslinked nanoparticles, worm-like micelles with an average length of 581 nm mediated the highest gene expression in the liver, with a level comparable to that achieved with hydrodynamic injection of plasmid DNA, which is considered the benchmark for liver-targeted gene delivery.[23] This gene expression level was 126-fold higher than for rod-like micelles with an average length of 130 nm, and 1,680-fold higher than for spherical micelles (Fig. 4g,h). Although the detailed mechanisms

responsible for such a strong variation in efficiency remain to be elucidated, the markedly higher transgene expression by worm-like particles may be related to the higher stability and lower macrophage uptake of worm-like or rod-like micelles.[5,7] We are presently characterizing cell-specific uptake by hepatocytes and Kupffer cells as well as *in vivo* biodistribution of these shaped nanoparticles.

Conclusions

This study demonstrates for the first time the shape tunability of DNA/PEG-*b*-polycation micellar nanoparticles by controlling solvent polarity, and the feasibility of preparing a series of highly uniform DNA nanoparticles with *different* shapes using the *same* polymer as condensing agent. Unlike shaped particles in earlier studies, here the DNA serves as an active payload and as a shape template. The resulting nanoparticles have a near-neutral zeta potential and surround the DNA with a protective polymeric corona. Moreover, they closely mimic the typical shapes (spherical, rod-like, and worm-like morphologies), sizes (20 to 80 nm in diameter, hundreds of nm in length for worm-like micelles), and physical features (flexible worm- and rod-like structures, and hydrated surfaces) of viral particles. Due to the difficulty of transforming the shape of viral particles, the role of shape in determining viral transport properties and bioactivities remains a mystery to date. Our sequence of synthetic nanoparticles of different shapes may provide a model system that makes it possible to address this question.

Experimental

Preparation of PEG-b-PPA/DNA micellar nanoparticles in DMF–water mixtures

VR1255 plasmid DNA (6.4 kb, encoding firefly luciferase driven by cytomegalovirus promoter, 25 μg) was first dissolved in 250 μl DI water or DMF–water mixtures with different DMF-to-water volumetric ratios ranging from 0:1, 3:7, 5:5 to 7:3 (v/v). PEG_{10K}-*b*-PPA_{4K} polymer (340.6 μg, corresponding to an N/P ratio of 8) was also dissolved in 250 μl of the same solvent and mixed with the plasmid DNA solution. The mixture was vortexed for 30 s, and then incubated at room temperature for 24 h before characterization. For TEM analysis, micelle samples were deposited on a TEM grid, stained with 2% uranyl acetate solution, and imaged on a Tecnai FEI-12 electron microscope. TEM images were analyzed with Image J 1.43.

Modeling of PEG-b-PPA/DNA complexation

Molecular dynamics simulations were performed of a semiflexible ring anionic polyelectrolyte and block copolymers comprised of a cationic block and a neutral block. All polymers were coarse-grained as bead–spring chains, placed in an implicit solvent that acted as a dielectric medium. Variation in solvent quality was represented by variation of the attractive strength of a Lennard-Jones potential acting between beads of the same type. Explicit counterions were added for electroneutrality and all electrostatic interactions were evaluated via Ewald summation.[12–14] With decreasing solvent quality, the de-correlation time between samples increased significantly. To ensure the equilibration of these systems, we employed parallel tempering in which the system was simulated in parallel at 12 (for solvent 1) to 92 (for solvent 4) closely spaced temperatures, permitting the system at the lowest (actual) temperature to overcome kinetic barriers through exchange with the simulations performed at higher temperatures.

Transformation of micelle shape by titrating solvent polarity

PEG_{10K}-*b*-PPA_{4K}/DNA micelles were first prepared in the presence of 7:3 (v/v) DMF–water mixture as described above (Fig. 1e). DI water was gradually titrated into 500 μl of

micelle solution with a syringe pump at a rate of 1 ml/h under stirring to achieve different DMF–water ratios (6:4, 5:5, 3:7, and 1:9, respectively).

Crosslinking of thiolated PEG-b-PPA/DNA micelles with different shapes

Thiolated PEG_{10K}-*b*-PPA_{4K} (Fig. S8) was used to prepare spherical micelles in the presence of 7:3 (v/v) DMF–water mixture, and the morphology of thiolated PEG_{10K}-*b*-PPA_{4K}/DNA micelles was transformed by titrating DI water as described above (Fig. S9). After transformation, the micelles were incubated at room temperature for 24 h and then subjected to aerial oxidation for 48 h under stirring (Fig. S10). DMF was then removed by dialyzing the micelle solution against DI water using dialysis tubing with MWCO of 3,500 for another 24 h.

In vivo transfection efficiency of crosslinked PEG-b-PPA/DNA micelles with different shapes via intrabiliary infusion

Animal studies were conducted under an animal protocol that was approved by the Johns Hopkins School of Medicine Institutional Animal Care and Use Committee (IACUC # RA09A447). Wistar rats (female, 6–8 weeks, 200–300 g) were anesthetized with intraperitoneal (*i.p.*) injection of Ketamine (100 mg/kg) and Xylazine (10 mg/kg). Four ml of crosslinked PEG_{10K}-b-PPA_{4K}/DNA micelles with different shapes containing 20 μg VR1255 DNA in 5% glucose solution were infused through the bile duct over 20 min with a syringe pump through a 33-gauge needle that was inserted into the common bile duct. Stitches with 10-O nylon suture were used to close the needle hole, if needed. At 4 h after infusion, the rat was anesthetized and given 1 ml of D-luciferin solution (*i.p.* 30 mg/ml). The rat was then imaged on an IVIS Spectrum Imaging System. The bioluminescence signal was collected for 1 min, and the level of luciferase expression was expressed as the total photon counts per second in the region of interest.

Supplementary Material

Refer to Web version on PubMed Central for supplementary material.

Acknowledgments

Funding for this study was partially provided by NIH grants R01GM073937, R01DK068399, R21EB013274, and U54CA151838, and NSF grant DMR-1006430, as well as a pilot grant from the Institute of NanoBioTechnology at Johns Hopkins University. We thank J. Michael McCaffery at the Integrate Imaging Center at Johns Hopkins University and the W. M. Keck College of Engineering Electron Microscopy Lab at the University of Delaware for providing support on TEM and cryo-TEM imaging, and the Quest high-performance computing facility at Northwestern University.

References

1. Pack DW, Hoffman AS, Pun S, Stayton PS. Nat Rev Drug Discov. 2005; 4:581. [PubMed: 16052241]
2. Davis ME. Curr Opin Biotechnol. 2002; 13:128. [PubMed: 11950563]
3. Harada-Shiba M, Yamauchi K, Harada A, Takamisawa I, Shimokado K, Kataoka K. Gene Ther. 2002; 9:407. [PubMed: 11960317] Itaka K, Kataoka K. Curr Gene Ther. 2011; 11:457. [PubMed: 22023475]
4. a) Chithrani BD, Ghazani AA, Chan WCW. Nano Lett. 2006; 6:662. [PubMed: 16608261] b) Gratton SEA, Ropp PA, Pohlhaus PD, Luft JC, Madden VJ, Napier ME, DeSimone JM. Proc Natl Acad Sci USA. 2008; 105:11613. [PubMed: 18697944] c) Zhang K, Fang H, Chen Z, Taylor JS, Wooley KL. Bioconjug Chem. 2008; 19:1880. [PubMed: 18690739]
5. Geng Y, Dalhaimer P, Cai SS, Tsai R, Tewari M, Minko T, Discher DE. Nat Nanotechnol. 2007; 2:249. [PubMed: 18654271]

6. Decuzzi P, Pasqualini R, Arap W, Ferrari M. Pharm Res. 2009; 26:235. [PubMed: 18712584]
7. Arnida, Janat-Amsbury MM, Ray A, Peterson CM, Ghandehari H. Eur J Pharm Biopharm. 2011; 77:417. [PubMed: 21093587]
8. Chauhan VP, Popovic Z, Chen O, Cui J, Fukumura D, Bawendi MG, Jain RK. Angew Chem Int Ed. 2011; 50:11417.
9. Mao HQ, Leong KW. Adv Genet. 2005; 53:275. [PubMed: 16240998]
10. Jiang X, Dai H, Ke CY, Mo X, Torbenson MS, Li ZP, Mao HQ. J Control Release. 2007; 122:297. [PubMed: 17640758]
11. Jiang X, Zheng Y, Chen HH, Leong KW, Wang TH, Mao HQ. Adv Mater. 2010; 22:2556. [PubMed: 20440698]
12. Guáqueta C, Luijten E. Phys Rev Lett. 2007; 99:138302. [PubMed: 17930645]
13. Hsiao PY, Luijten E. Phys Rev Lett. 2006; 97:148301. [PubMed: 17155292]
14. Sanders LK, Xian WJ, Guáqueta C, Strohman MJ, Vrasich CR, Luijten E, Wong GCL. Proc Natl Acad Sci USA. 2007; 104:15994. [PubMed: 17911256]
15. Rudnick J, Gaspari G. Science. 1987; 237:384. [PubMed: 17794340]
16. Guo L, Luijten E. Macromolecules. 2003; 36:8201.
17. Bloomfield VA. Curr Opin Struct Biol. 1996; 6:334. [PubMed: 8804837]
18. Ke FY, Luu YK, Hadjiargyrou M, Liang DH. Plos One. 2010; 5:e13308. [PubMed: 20949017]
19. Daoud M, Cotton JP. J Phys-Paris. 1982; 43:531.
20. a) Shen HW, Eisenberg A. J Phys Chem B. 1999; 103:9473.b) Cui HG, Chen ZY, Zhong S, Wooley KL, Pochan DJ. Science. 2007; 317:647. [PubMed: 17673657]
21. Bauhuber S, Hozsa C, Breunig M, Gopferich A. Adv Mater. 2009; 21:3286. [PubMed: 20882498]
22. Dai H, Jiang X, Tan GC, Chen Y, Torbenson M, Leong KW, Mao HQ. Int J Nanomedicine. 2006; 1:507. [PubMed: 17369870]
23. Herweijer H, Wolff JA. Gene Ther. 2007; 14:99. [PubMed: 17167496]

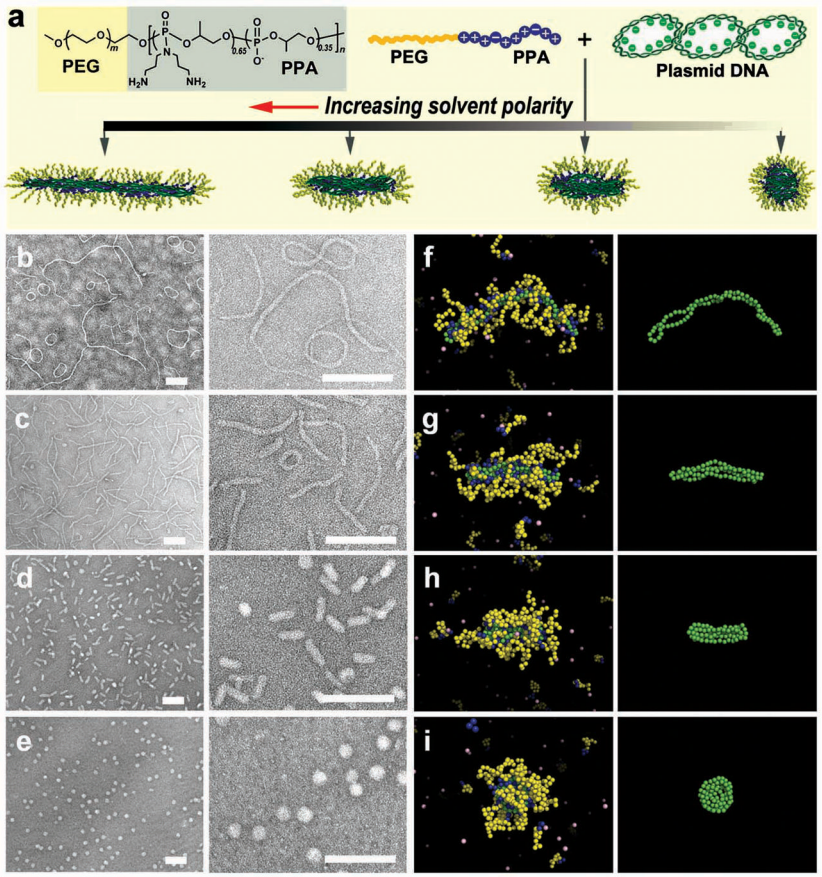

Figure 1.

Assembly of micellar nanoparticles with different shapes by condensing DNA with PEG_{10K}-*b*-PPA_{4K} block copolymer in solvents with different polarities. (**a**) Structure of PEG_{10K}-*b*-PPA_{4K} and schematic illustration of its assembly with DNA. (**b**–**e**) Morphologies of PEG-*b*-PPA/DNA micelles prepared in deionized water (**b**), 3:7 (v/v) (**c**), 5:5 (v/v) (**d**), and 7:3 (v/v) (**e**) DMF–water mixtures at an N/P ratio (ratio of primary amino groups in PPA block of the copolymer to phosphate groups in DNA) of 8. All scale bars represent 200 nm. (**f**–**i**) Representative images of PEG-*b*-PPA/DNA micelles obtained in molecular dynamics simulations corresponding to the conditions shown in panels (**b**–**e**). DNA is represented in green and the PEG and PPA blocks in yellow and blue, respectively. Monovalent counterions are depicted in pink. For clarity, the panels in the right-most column show the conformations of the plasmid DNA *within* the corresponding micelles depicted in panels (**f**–**i**).

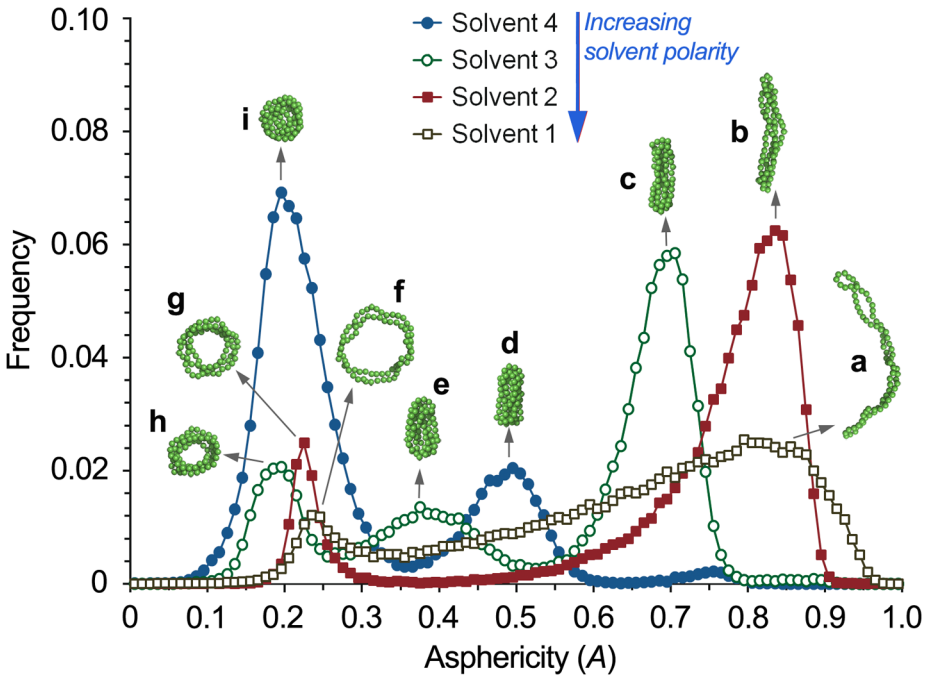

Figure 2.

Frequency distribution of the asphericity (characterizing particle shape) of PEG-*b*-PPA/DNA micelles in Solvents 1 (grey open squares), 2 (red solid squares), 3 (green open circles), and 4 (blue solid circles), representing various water–DMF mixtures. Insets (**a**–**i**) show snapshots of representative DNA conformations within micelles of asphericities corresponding to the peaks of the frequency distributions. Copolymers and residue counterions have been omitted for clarity.

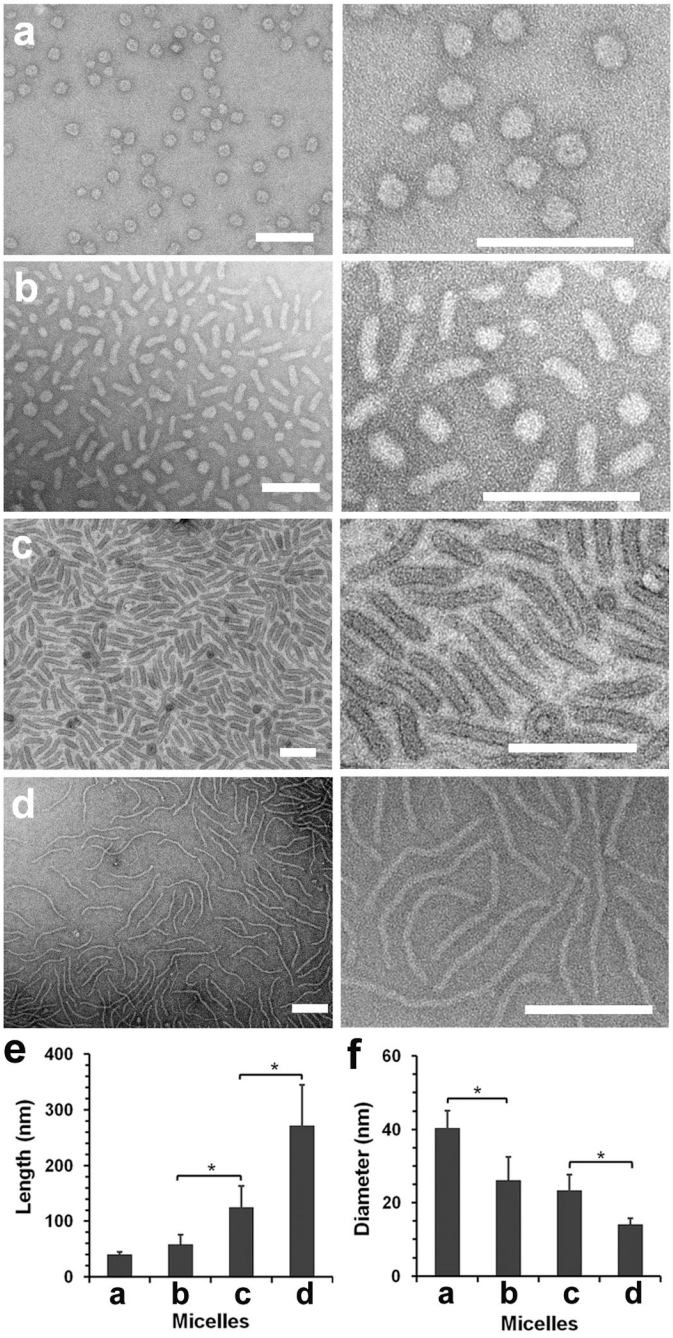

Figure 3.

Morphological transition of PEG-*b*-PPA/DNA micelles induced by increasing solvent polarity. (**a**–**d**) TEM images of transformed micelles obtained in 6:4 (v/v) (a), 5:5 (b), 3:7 (c), and 1:9 DMF–water mixture (d). (**e** and **f**) Average lengths and diameters of transformed micelles prepared at different DMF fractions as shown in panels (**a**–**d**). Plot shows mean ± standard deviation ($n > 100$, $^{*}p < 0.01$; Student's t-test).

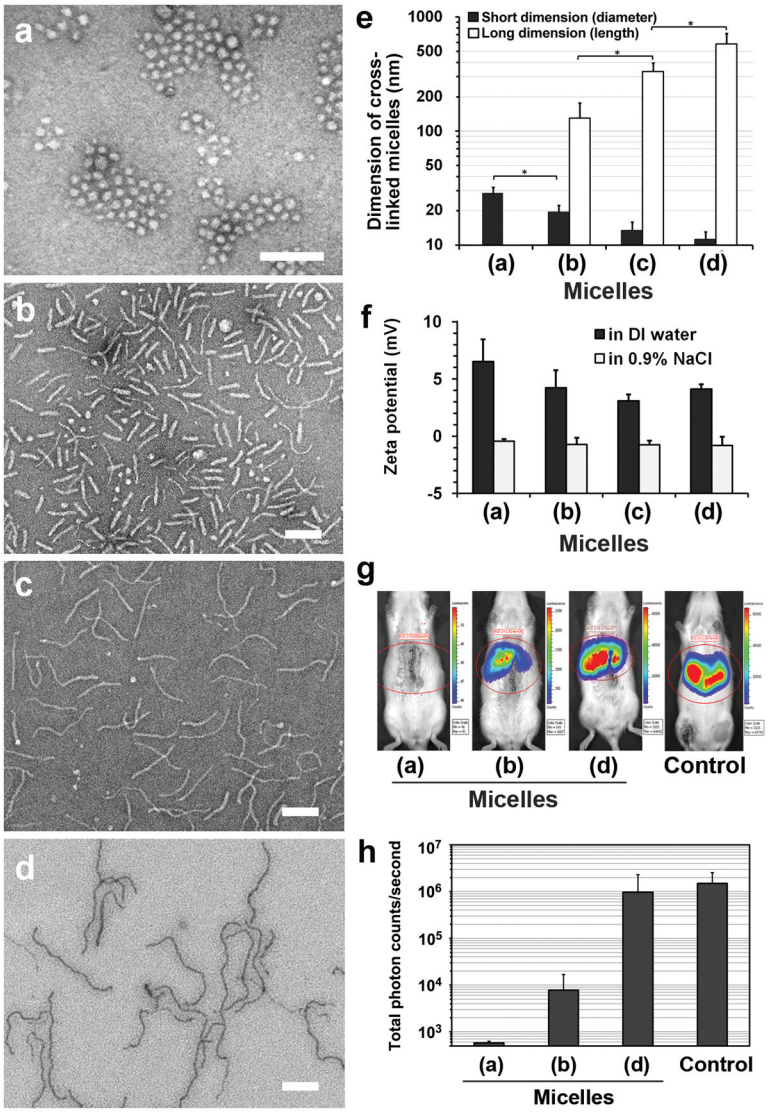

Figure 4.

Preservation of the morphologies of PEG-*b*-PPA/DNA micelles by reversible disulfide crosslinking and shape-dependent gene transfection efficiency *in vivo*. (**a**–**d**) TEM images of the crosslinked micelles initially obtained in 7:3 (v/v) (**a**), 5:5 (**b**), 4:6 (**c**), and 1:9 DMF–water mixtures (**d**). All scale bars represent 200 nm. (**e**) The average lengths and diameters of crosslinked micelles as shown in (**a**) through (**d**). Plot shows mean ± standard deviation ($n > 100$, $^{*}p < 0.01$; Student's t-test). (**f**) Average zeta potentials of the micelles in water and isotonic sodium chloride solution. Plot shows mean ± standard deviation ($n = 3$). (**g**) Distribution of luciferase expression at 4 h after intrabiliary infusion of PEG-*b*-PPA/DNA micelles with spherical (**a**), rod-like (**b**), and worm-like (**d**) shapes, characterized with *in vivo* bioluminescence imaging. The control group is a benchmark expression level obtained by the hydrodynamic infusion of plasmid DNA (See Supporting Information). (**h**) Quantitative comparison of luciferase expression in rat liver at 4 h after infusion for the same set of micelles. Plot shows mean ± standard deviation ($n = 3$). Background reading for this assay was 3.5×10^2 total photon counts per second.